Acta Crystallographica Section D
Biological Crystallography
ISSN 0907-4449

Atomic resolution structures of the c-Src SH3 domain in complex with two high-affinity peptides from classes I and II

Julio Bacarizo and Ana Camara-Artigas*

Department of Chemistry and Physics, University of Almería, Agrifood Campus of International Excellence (ceiA3), Carretera de Sacramento, 04120 Almería, Spain

Correspondence e-mail: acamara@ual.es

Received 13 December 2012
Accepted 15 January 2013

PDB References: Src-SH3-T98D–APP12, 4hvu; Src-SH3-T98E–APP12, 4hvv; Src-SH3-T98E–VSL12, 4hvw

The atomic resolution crystal structures of complexes between the SH3 domain of the c-Src tyrosine kinase and two high-affinity peptides belonging to class I and class II have been solved. The crystals of the Thr98Asp and Thr98Glu mutants in complex with the APP12 peptide (APPLPPRNRPRL) belonged to the trigonal space group $P3_121$ and in both cases the asymmetric unit was composed of one molecule of the SH3–APP12 complex. The crystals of the Thr98Glu mutant in complex with the VSL12 peptide (VSLARRPLPLP) belonged to the trigonal space group $P3_221$ and the asymmetric unit was also composed of a single molecule of the SH3–VSL12 complex. All crystals were obtained in the presence of PEG 300 under the same conditions as reported for the intertwined dimeric structure of the c-Src SH3 domain, but the presence of the peptide stabilizes the monomeric form of the domain. These structures allow a detailed analysis of the role of salt bridges, cation–π interactions and hydrogen bonds in the binding of proline-rich motifs to the c-Src SH3 domain. Moreover, these crystallographic structures allow the role of water molecules in the binding of these motifs to the c-Src SH3 domain to be studied for the first time.

1. Introduction

The SH3 domain is one of the most widely present structural modular domains in proteins and it is also among the best characterized (Cesareni *et al.*, 2006; Kay, 2012). These domains are present in tyrosine kinases, in which they play an important role in the regulation of the enzymes through transient interactions with the linker region between the SH2 domain and the kinase domain, which contains the canonical P*xx*P binding motif of the SH3 domains. The importance of this regulation mechanism in cellular function is underscored by the fact that tyrosine kinases comprise the largest group of oncoproteins (Rodrigues & Park, 1994). In addition, these SH3 domains can also interact with other proteins containing proline-rich motifs (PRMs) with the consensus motif P*xx*P. Upon binding, the PRMs adopt the polyproline type II helical conformation (PII helix) and the two prolines flanked by hydrophobic residues are buried in two different hydrophobic pockets on the surface of the SH3 domain. The symmetry of the PII helix allows the binding of the peptide in different orientations with respect to the SH3 binding surface (Feng *et al.*, 1994), and the binding orientation of the peptide can be determined by the presence of charged residues flanking the consensus motif P*xx*P (Feng *et al.*, 1995). These charged amino acids can form salt bridges with those located within the third pocket formed by the RT loop and the n-Src loop. PRMs with sequences (K/R)*xx*P*xx*P and *x*P*xx*P*x*(K/R) correspond to class I and class II motifs, respectively.

© 2013 International Union of Crystallography
Printed in Singapore – all rights reserved

To date, no crystallographic structures of the SH3 domain of the c-Src tyrosine kinase in complex with PRMs are available. Structures of the c-Src SH3 domain complexed with APP12 (APPLPPRNRPRL) and VSL12 (VSLARRPLPLP) have previously been determined by multidimensional NMR spectroscopy (Feng *et al.*, 1994). These peptides were obtained from biased phage display libraries and the dissociation constants obtained by means of fluorescence techniques were 1.2 and 0.45 μ*M* for APP12 and VLS12, respectively (Feng *et al.*, 1995). The NMR structures of the two complexes allowed the origin of the high-affinity binding of APP12 and VSL12 to the c-Src SH3 domain and the specificity determinants outside the core sequence to be analysed for the first time. However, the importance of water molecules buried in the binding interface in the energetics of the binding of PRMs to SH3 domains has recently been reported (Palencia *et al.*, 2010), but NMR structures do not provide information about the solvent. This key role of the solvent was proposed taking into account the thermodynamic signature of the binding observed in most calorimetric titrations of SH3 domains with PRMs: negative binding enthalpies partially compensated by unfavourable entropic contributions (Palencia *et al.*, 2004). This would be an unexpected result considering the hydrophobic nature of the binding site of the SH3 domains and the PRMs. Whereas no crystallographic structures of complexes of the c-Src SH3 domain are available to date, we have recently solved the structures of the Fyn SH3 domain in complex with the NS5A and VSL12 peptides (Martin-Garcia, Luque *et al.*, 2012). This domain, which shows high homology to the c-Src SH3 domain, does not have water molecules buried at the binding interface of the complex. Consequently, these crystallographic structures suggested that further additional interactions would account for the unexpected thermodynamic signature.

In order to determine whether the lack of water molecules at the binding site is a special feature of the Fyn SH3 domain or whether it is common to the Src family of tyrosine kinases, we have solved crystallographic structures of the c-Src SH3 domain in complex with two different high-affinity peptides belonging to classes I and II. These are the first crystallographic structures of the c-Src SH3 domain in complex with PRMs. Additionally, these structures have been solved using the first atomic resolution data measured at ALBA, the Spanish synchrotron-radiation facility (Barcelona, Spain; Benach *et al.*, 2012). The structures were solved from crystals of two different mutants of the c-Src SH3 domain: Thr98Asp and Thr98Glu. This threonine is placed in the RT loop next to the aspartate which forms a salt bridge to the arginine residue of the peptide and drives the orientation of the bound PRM. While the aspartate residue Asp99 is well conserved among the members of the Src family of tyrosine kinases, Thr98 is changed to an aspartate in Fyn tyrosine kinase (Thr98Asp; Asp99 in the Fyn SH3 domain sequence; PDB entry 3ua6; Martin-Garcia, Luque *et al.*, 2012) and to glutamate in Yes tyrosine kinase (Thr98Glu; Glu108 in the Yes SH3 domain sequence; PDB entry 2hda; Martín-García *et al.*, 2007). The presence of a negatively charged residue next to Asp99 might affect the electrostatic interaction of this residue with the arginine residues present in the flanking sequences of the APP12 (APPLPP**R**N**R**P**R**L) and VSL12 (VSLA**RR**PLPLP) peptides (Feng *et al.*, 1995). Because of the role played by the RT loop in the binding process, we have studied the effect of these mutations in the structures of their complexes with two high-affinity peptides from classes I and II containing additional positively charged residues in the flanking sequences.

2. Materials and methods

2.1. Cloning, expression and purification of chicken c-Src SH3 domain

The plasmid pET15b containing the chicken c-Src SH3 domain gene was a generous gift from Dr E. Freire (John Hopkins University, USA). The plasmid was expressed in *Escherichia coli* strain BL21 (DE3) (Novagen) with an N-terminal 6×His tag and an engineered thrombin cleavage site. The mutants of the chicken c-Src SH3 domain were a generous gift from Dr I. Luque (Granada University, Spain). These mutants were obtained from the previous plasmid by punctual mutation using the QuikChange Site-Directed Mutagenesis Kit (Stratagene). The protein was purified using the standard protocol and its concentration was determined as described previously (Cámara-Artigas, Martín-García *et al.*, 2009).

2.2. Peptide ligands

The peptides APP12 (APPLPPRNRPRL) and VSL12 (VSLARRPLPLP) were purchased from JPT Innovative Peptide Solutions (Germany). The peptides were synthesized in solid phase in an MPS column and were acetylated and amidated at their N-termini and C-termini, respectively. Their molecular weights were confirmed by mass spectrometry and the peptide purity (>95%) was assessed by analytical HPLC. Peptide stock solutions were prepared in water and their concentrations were determined as described previously (Scopes, 1974).

2.3. Dynamic light scattering (DLS)

DLS experiments were performed in a Zetasizer Nano (Malvern Instruments, UK) with an Avalanche photodiode detector (quantum efficiency of >50% at 633 nm), a class I compliant laser and automatic laser attenuation, and the data from the DLS experiments were analyzed using the *Zetasizer* software (Malvern Instruments, UK). DLS measurements were carried out in a 12 μl quartz sample cuvette (low-volume quartz ZEN2112) thermostatted at 298 K. Each hydrodynamic radius (R_h) value reported is the average of 15 measurements. Before performing the measurements all protein samples were filtered through 0.2 μm filters (IC Millex-LG, Millipore) and centrifuged for 45 min at 14 000 rev min^{-1} in order to remove any aggregates and dust. Immediately before measurement, the protein solutions were sonicated for 1 min to remove bubbles.

Table 1
Data-collection and refinement statistics.

Values in parentheses are for the highest resolution bin.

	Src-SH3-T98D–APP12	Src-SH3-T98E–APP12	Src-SH3-T98E–VSL12
Wavelength (Å)	0.98	0.94	0.98
Resolution range (Å)	19.07–0.98 (1.02–0.98)	19.10–1.10 (1.14–1.10)	18.72–0.98 (1.02–0.98)
Space group	$P3_121$	$P3_121$	$P3_221$
Unit-cell parameters (Å, °)	$a = b = 31.50$, $c = 106.71$, $\alpha = \beta = 90$, $\gamma = 120$	$a = b = 31.59$, $c = 106.69$, $\alpha = \beta = 90$, $\gamma = 120$	$a = b = 37.44$, $c = 85.62$, $\alpha = \beta = 90$, $\gamma = 120$
Total reflections	169003 (2555)	239998 (4855)	167748 (2766)
Unique reflections	35466 (3060)	24823 (1852)	40037 (3450)
Multiplicity	4.8 (1.8)	9.6 (5.5)	4.2 (1.6)
Completeness (%)	97.60 (85.57)	95.34 (72.20)	98.12 (85.29)
Mean $I/\sigma(I)$	27.52 (4.56)	19.05 (2.75)	17.72 (3.75)
Wilson B factor (Å^2)	10.85	11.80	9.43
$R_{\rm merge}$†	0.034 (0.169)	0.064 (0.606)	0.046 (0.161)
R factor	0.145 (0.182)	0.144 (0.231)	0.145 (0.204)
$R_{\rm free}$	0.160 (0.178)	0.156 (0.263)	0.149 (0.223)
No. of atoms	1167	1143	1316
Macromolecules	547	545	636
Ligands	14	8	8
Waters	89	73	89
No. of protein residues	68	67	74
R.m.s.d., bonds (Å)	0.011	0.009	0.009
R.m.s.d., angles (°)	1.55	1.21	1.47
Ramachandran favoured‡ (%)	100	100	99
Ramachandran outliers‡ (%)	0	0	0
Clashscore	7.37	5.59	6.29
Average B factor (Å^2)	18.00	18.90	12.40
Macromolecules	15.50	16.60	10.70
Solvent content (%)	32.00	34.40	24.50

† $R_{\rm merge} = \sum_{hkl}\sum_i |I_i(hkl) - \langle I(hkl)\rangle| / \sum_{hkl}\sum_i I_i(hkl) \sum_{hkl}\sum_i I_i(hkl)$, where $I_i(hkl)$ is the ith observation of reflection hkl and $\langle I(hkl)\rangle$ is the weighted average intensity for all i observations of reflection hkl. ‡ Statistics from *PROCHECK* (Laskowski *et al.*, 1993).

2.4. Cross-linking experiments

c-Src SH3 domain aliquots (5–13 mg ml^{-1}) were prepared in the presence or absence of 5% PEG 300 and with or without peptide in 100 m*M* acetate buffer pH 5. Protein samples (75 µl) were incubated with 6 µl 0.2 *M* glutaraldehyde and 10 µl 1 *M* sodium borate for 20 s. The experiments were conducted at room temperature; the reaction was stopped by the addition of 7.5 µl 1 *M* sodium borohydride. Cross-linking experiments were analyzed by SDS–PAGE in a Mini Protean Tetra Cell (Bio-Rad) using a voltage of 200 V (60 mA): 10 µl of the cross-linked sample was diluted in 30 µl SDS–PAGE sample buffer [62.5 m*M* Tris–HCl pH 6.8, 2% SDS, 10 m*M* β-mercaptoethanol, 10%(*v*/*v*) glycerol, 0.05%(*w*/*v*) bromophenol blue]. After boiling, samples were loaded onto 16% acrylamide gels. The gels were stained with Coomassie Blue R-250 staining solution [40%(*v*/*v*) ethanol, 20%(*v*/*v*) acetic acid, 0.1%(*w*/*v*) Coomassie Blue R-250]. Excess staining solution was removed with a destaining solution consisting of 25%(*v*/*v*) ethanol, 7.5%(*v*/*v*) acetic acid.

2.5. Size-exclusion chromatography

The oligomerization of the c-Scr SH3 domain was analyzed by size-exclusion chromatography using a HiLoad 16/60 Superdex 75 column (GE Healthcare). The column was equilibrated with 100 m*M* sodium acetate buffer pH 5.0. Chromatography was performed using an ÄKTA FPLC (GE Healthcare) at a flow rate of 0.3 ml min^{-1}. Protein elution was monitored at 280 nm.

2.6. Protein structure

2.6.1. Protein crystallization. Crystals of the c-Src SH3 domain (Src-SH3) in complex with the high-affinity peptides APP12 and VSL12 were obtained by the vapour-diffusion technique using a sitting-drop setup. Briefly, the protein complex was prepared by mixing c-Src SH3 at 10 mg ml^{-1} in 10 m*M* Tris buffer pH 8.0 with the APP12 or VSL12 peptide in a 1:2 molar ratio. The next day, 6 µl droplets were prepared by mixing 3 µl complex solution and 3 µl reservoir solution. The mixture was vapour-equilibrated against 1 ml reservoir solution. The best crystals were obtained with 1.7 *M* ammonium sulfate, 10% PEG 300, 10% glycerol, 0.1 *M* sodium acetate pH 5 for the APP12 complexes and 1.7 *M* ammonium sulfate, 5% PEG 300, 10% glycerol, 0.1 *M* sodium acetate pH 5 for the VSL12 complex. Crystals typically appeared within 1–2 months. For data collection, the crystals were looped and cooled in liquid nitrogen. X-ray diffraction data were collected in a cold nitrogen stream maintained at 110 K on the XALOC beamline at the ALBA Synchrotron Radiation Facility at a wavelength of 0.98 Å using a PILATUS detector (Src-SH3-T98D–APP12 and Src-SH3-T98E–VSL12) and on beamline ID14-4 at the European Synchrotron Radiation Facility (ESRF) at a wavelength of 0.94 Å using an ADSC Quantum Q315r detector (Src-SH3-T98E–APP12). The data were indexed and integrated with the program *XDS* (Kabsch, 2010*a*,*b*). Data scaling was performed using the program *AIMLESS* (Evans, 2011) from the *CCP*4 suite (Winn *et al.*, 2011). The crystallographic parameters and data-collection statistics are listed in Table 1.

2.6.2. Structure resolution and refinement. Solution and refinement of the structure was performed using the *PHENIX* suite (Adams *et al.*, 2010). Molecular-replacement phasing using the *AutoMR* feature of *PHENIX* (Afonine *et al.*, 2012) was performed using the coordinates of a monomer generated from the intertwined structure of the c-Src SH3 Gln128Arg mutant (PDB entry 3fj5; Cámara-Artigas, Martín-García *et al.*, 2009) as a model. The model was built without the n-Src loop, which acts as a hinge loop in the intertwined structure, and without ligand and water molecules. The n-Src loop was built using the *Phase and Build* feature of *PHENIX* (Terwilliger *et al.*, 2008). This is the only problematic region in the VSL12

complex and automated rebuilding was repeated several times. Finally, the best model was used in manual building performed using the resulting σ_A-weighted ($2F_o - F_c$) and ($F_o - F_c$) electron-density maps and the program *Coot* (Emsley & Cowtan, 2004; Emsley *et al.*, 2010). In the VSL12 complex, the refined solution shows electron density to model the loop residues 111–114 in two different conformations. H atoms were included in the model using *phenix.ready_set*.

Water and some molecules from the precipitant solution were identified in the electron-density difference maps. Water molecules were modelled automatically using *phenix.refine* in *PHENIX* (Afonine *et al.*, 2012) and were subsequently manually inspected in difference electron-density maps in *Coot*. Final cycles of refinement were performed using anisotropic *B* factors. The quality of the structure was checked using *MolProbity* (Chen *et al.*, 2010) and *PROCHECK* (Laskowski, 1993). Refinement statistics are collected in Table 1.

Structure superposition and r.m.s.d. calculations were performed using the *CCP*4 module *LSQKAB* (Kabsch, 1976). Protein interfaces in the crystal were characterized using the *PISA* server (Krissinel, 2011). Distances between amino acids and accessible surface areas (ASAs) were calculated using the *CONTACT* and *AREAIMOL* programs from the *CCP*4 suite (Winn *et al.*, 2011), respectively.

The coordinates and structure factors were deposited in the Protein Data Bank (PDB) as entries 4hvu, 4hvv and 4hvw for the crystallographic structures of the Src-SH3-T98D–APP12, Src-SH3-T98E–APP12 and Src-SH3-T98E–VSL12 complexes, respectively.

3. Results

3.1. Crystal structure of the c-Src SH3 domain–APP12 complex

The structures of two c-Src SH3 domain mutants, Thr98Asp and Thr98Glu, have been solved at atomic resolution in complex with the high-affinity synthetic peptide APP12 (Feng *et al.*, 1995) from crystals belonging to space group $P3_121$: c-Src-SH3-T98D–APP12 (0.98 Å resolution) and c-Src-SH3-T98E–APP12 (1.1 Å resolution). The asymmetric unit is composed of a single molecule of the SH3–APP12 complex. As reported previously, the SH3 structural motif shows a β-barrel fold which consists of five β-strands arranged as two tightly packed antiparallel β-sheets with a shallow groove formed by the RT and n-Src loops (Musacchio *et al.*, 1994). The APP12 peptide is placed in this groove and the peptide shows the PPII conformation and the class II orientation expected from its sequence [APPLPPRNRPRL; class II, *x*P*xx*P*x*(K/R), where *x* represents any amino acid]. In both structures the occupancies of all the residues in the peptide are 1, except for some atoms of the $Arg9_{APP12}$ side chain. The last two carboxy-terminal residues of the peptide do not have sufficient electron density to be modelled. The amino- and carboxy-terminal residues of the SH3 domain also show high flexibility and have not been modelled. Fig. 1 shows the interactions established by the APP12 peptide using the *LigPlot+* program (Laskowski & Swindells, 2011) in *PyMOL* (DeLano, 2002).

At the binding site, the hydrophobic pockets formed by Tyr90–Tyr136 and Tyr92–Tyr136–Trp118 are occupied by the residues Ala1-Pro2 and Leu4-Pro5, respectively (Fig. 1*a*). The

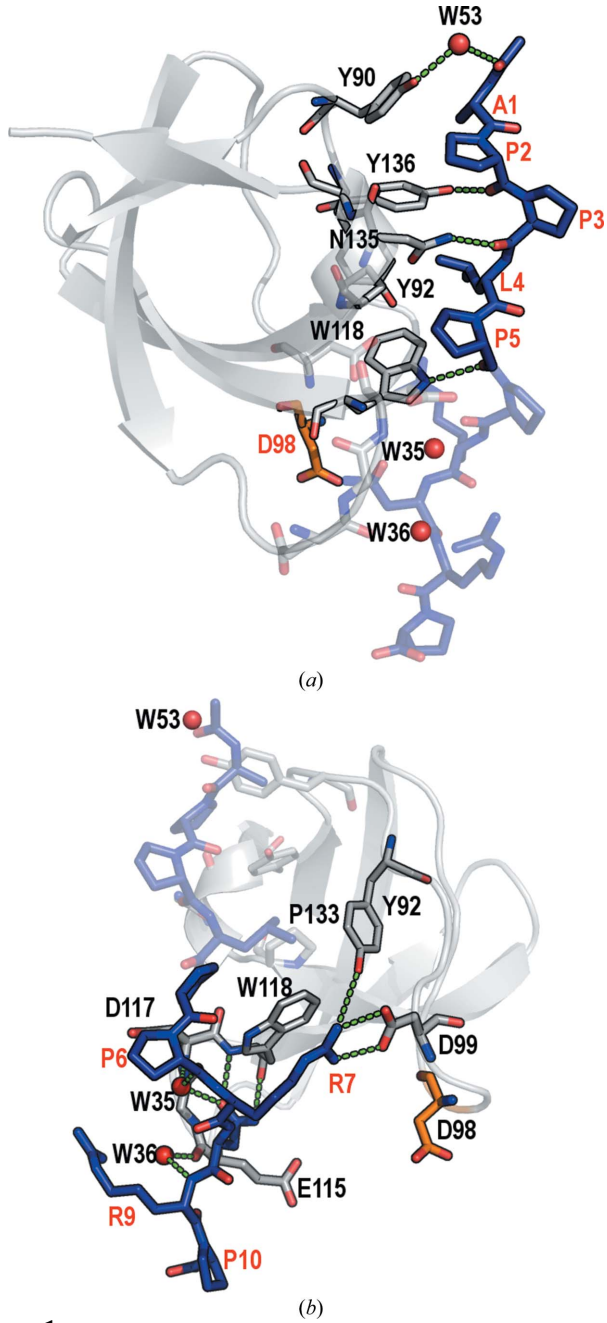

Figure 1
Hydrogen-bond interactions (green dashed lines) involved in the binding of the APP12 peptide (blue) to the c-Src SH3 domain Thr98Asp mutant (grey). The binding site with (*a*) the canonical motif P*xx*P and (*b*) the flanking sequence are shown in detail. The SH3 domain is shown in cartoon representation and the residues involved in the binding interactions are represented as sticks. The modified residue, Thr98Asp (orange), is not involved in the binding interactions. Water molecules in the binding site are shown as spheres. The figure was created using the *LigPlot+* program (Laskowski & Swindells, 2011) in *PyMOL* (DeLano, 2002) with the default values for the donor–acceptor distances and angles.

third pocket, formed by Trp118–Tyr131 and the residues in the n-Src and RT loops, binds the flanking sequence (Fig. 1*b*). This pocket is the most structurally diverse among the SH3 domains and forms the basis of their differential specificity (Kaneko *et al.*, 2011). In the Src family of tyrosine kinases this specificity is controlled by the formation of salt bridges between the charged residues of the peptide and the residues in the RT loop. In the Src-SH3–APP12 complex this salt bridge is formed between Asp99 and $Arg7_{APP12}$ and determines the orientation of the peptide. Additionally, the affinity of the peptide can be modulated by other interactions: Tyr92 forms a hydrogen bond to $Arg7_{APP12}$ (3.5 Å) and the guanidinium group of $Arg7_{APP12}$ is placed parallel to the aromatic ring of Trp118, forming a cation–π interaction (Fig. 1*b*).

Comparison of the structures of the APP12 complex of the Thr98Glu and Thr98Asp mutants shows that the mutation does not introduce significant changes (backbone r.m.s. deviation of 0.22 Å). Neither Asp98 nor Glu98 participate in contacts with the APP12 or other SH3 domain residues implicated in the binding (Fig. 1*b*).

3.2. Comparison of the c-Src SH3 domain–APP12 complex with previous structures

Comparison of our two crystallographic structures with the previously reported averaged minimized NMR structure of the Src-SH3–APP12 complex (PDB entry 1qwe; Feng *et al.*, 1995) reveals backbone r.m.s.d.s of 1.26 Å (Thr98Asp mutant) and 1.18 Å (Thr98Glu mutant) on superposition of the SH3 domain residues (Fig. 2). However, if the superposition is performed only with the residues of the peptide (1–10) the backbone r.m.s.d.s are 2.19 and 2.11 Å for the Thr98Asp and the Thr98Glu mutants, respectively. Additionally, while some minor differences are found in the n-Src and RT loops, surprisingly the highest differences between the crystallographic and NMR structures are found in the distal loop, which is located at the opposite side to the binding site. Comparison of the crystallographic c-Src-SH3–APP12 complexes with the unligated NMR structure (PDB entry 1srl; Yu *et al.*, 1993) results in backbone r.m.s. deviations of 2.21 Å (Thr98Asp mutant) and 2.14 Å (Thr98Glu mutant). The r.m.s.d. plot indicates that these differences arise as a

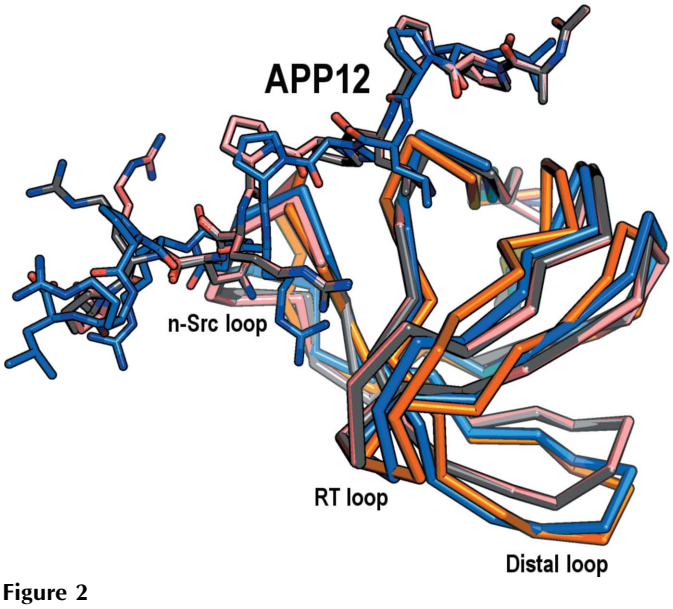

Figure 2
Superposition of the crystallographic APP12 complex of the c-Src SH3 domain (Thr98Asp, light pink; Thr98Glu, dark grey) with that solved using NMR (PDB entry 1qwe; blue) and the unligated structure (PDB entry 1srl; orange).

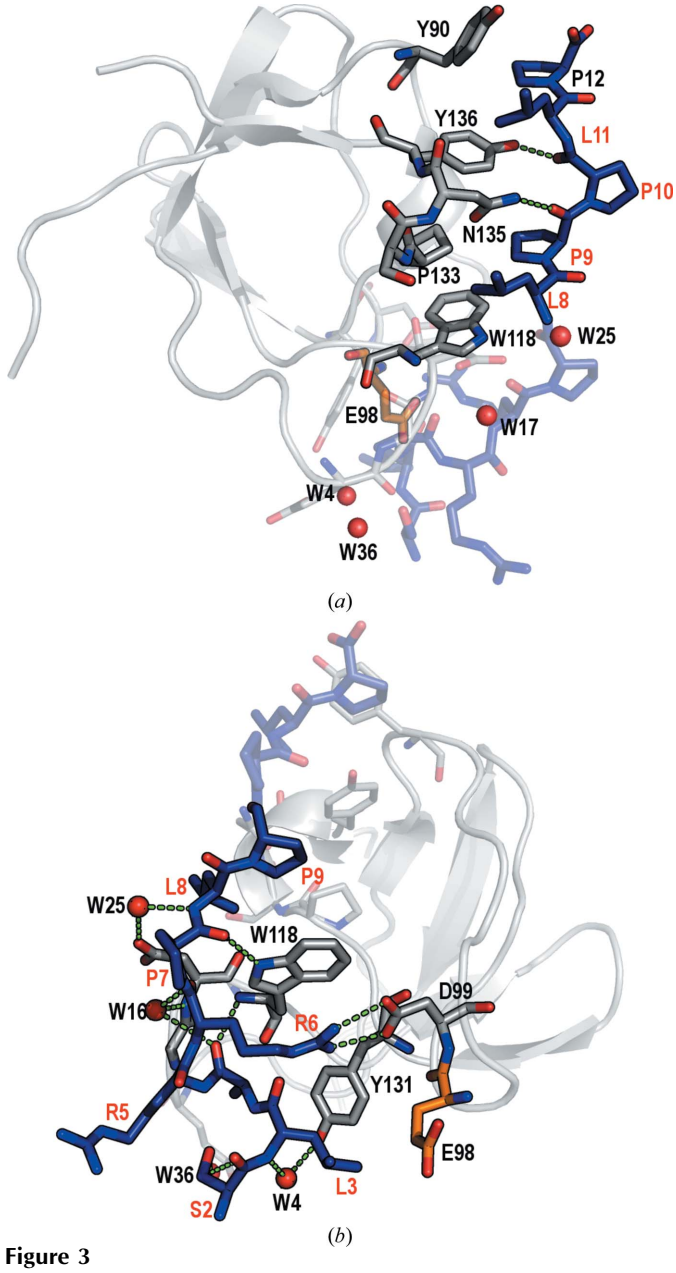

Figure 3
Hydrogen-bond interactions (green dashed lines) involved in the binding of the VSL12 peptide (blue) and the c-Src SH3 domain Thr98Glu mutant (grey). The binding site with (*a*) the canonical motif P*xx*P and (*b*) the flanking sequence are shown in detail. The SH3 domain is shown in cartoon representation and the residues involved in the binding interactions are represented as sticks. The modified residue, Thr98Glu (orange), is not involved in the binding interactions. Water molecules in the binding site are shown as spheres. The figure was created using the *LigPlot+* program (Laskowski & Swindells, 2011) in *PyMOL* (DeLano, 2002) with the default values for the donor–acceptor distances and angles.

consequence of displacement of the n-Src loop. In the peptide-bound structures this movement results in a more packed conformation which allows contacts between residues present in the n-Src and RT loops and those in the flanking sequence of the peptide. The same differences that are found between the crystallographic and the NMR complex structures in the position of the distal loop are also present in the unligated structure (Fig. 2).

To date, the only unligated crystallographic structure of the c-Src SH3 domain (PDB entry 3fj5; Cámara-Artigas, Martín-García *et al.*, 2009) appears in the asymmetric unit as an intertwined dimer which is stabilized by the binding of a low-molecular-weight PEG molecule. Superposition of the Src-SH3–APP12 crystallographic structures with the intertwined crystallographic structure of the unligated c-Src SH3 domain does not show differences in the position of the backbone atoms at the distal loop. We have also compared our structures with the SH3 domain present in the crystal structure of the inactivated form of chicken Src tyrosine kinase (PDB entry 2ptk; Williams *et al.*, 1997) and only minor differences are found in the conformation of the distal loop compared with our crystallographic structures.

All of the comparisons of crystallographic and NMR structures indicate that for both the ligated and unligated structures the c-Src SH3 domain shows the largest differences in the n-Src loop. This loop acts as the hinge loop that allows domain swapping to form an intertwined dimer and it is expected to have a large conformational flexibility, which is noticeable in the crystallographic structures of the complex by the high *B* factors determined for the residues belonging to this loop compared with the average value for the whole structure. In this way, the residues in the n-Src loop show *B* factors higher than 30 Å^2, while the *B* factors for the whole structure are 16.77 and 18.02 Å^2 for c-Src-SH3-T98D–APP12 and c-Src-SH3-T98E–APP12, respectively.

3.3. Crystal structure of the c-Src-SH3 domain–VSL12 complex

We have solved the structure of the c-Src SH3 domain Thr98Glu mutant complexed with the high-affinity synthetic peptide VSL12 at atomic resolution (0.98 Å). The overall fold is the same as that described for the APP12 complexes, but the crystals of this complex belonged to space group $P3_221$ and showed different unit-cell parameters (see Table 1). These crystals also contained a single molecule of the SH3–VSL12 complex in the asymmetric unit. The VSL12 peptide (VSLARRPLPLP) is placed in the shallow groove formed by the RT and n-Src loops with the expected PPII conformation and the class I orientation [class I, (K/R)*xx*P*xx*P, where *x* represents any amino acid]. Fig. 3 shows the interactions established by the VSL12 peptide obtained using the *LigPlot+* program (Laskowski & Swindells, 2011) and *PyMOL* (DeLano, 2002).

At the binding site, residues Leu11-Pro12 and Leu8-Pro9 interact with the hydrophobic pockets formed by Tyr90–Tyr136 and Tyr92–Tyr136–Trp118, respectively (Fig. 3*a*). In the third pocket, the flanking sequence of the VSL12 peptide forms a salt bridge between Arg6$_{VSL12}$ and Asp99, but in this case the interaction of the guanidinium group of Arg6$_{VSL12}$ with the aromatic ring of Trp118 (∼4.5 Å) is weaker than those observed in the APP12 complexes (∼3.5 Å) (Fig. 3*b*). The salt bridge between Arg6$_{VSL12}$ and Asp99, which drives the peptide orientation in its binding to the SH3 domain, is the main difference between the class I and II complexes. In this orientation, the position of the arginine residue causes

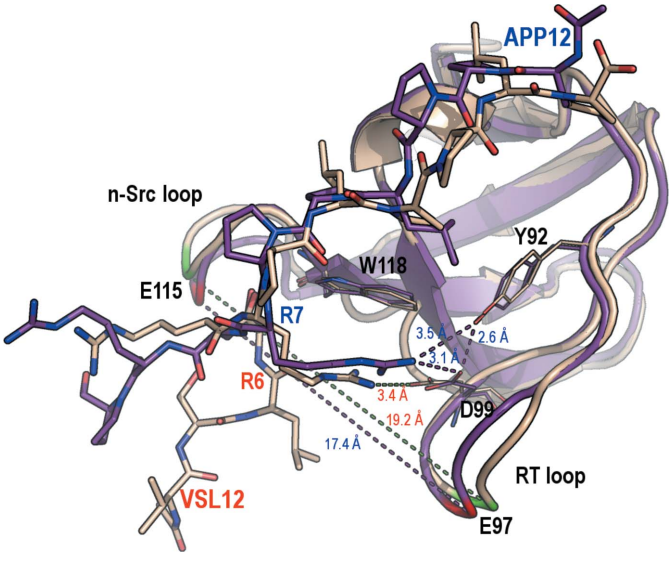

Figure 4
Superposition of the crystallographic structures of the APP12 (purple) and VSL12 (gold) complexes of the c-Src SH3 domain Thr98Glu mutant. Distances between residues are indicated in red and blue for the VSL12 and APP12 complexes, respectively. The position of Glu97 (at the tip of the RT loop) and Glu115 (at the tip of the n-Src loop) are indicated in red and green for the APP12 and VSL12 complexes, respectively.

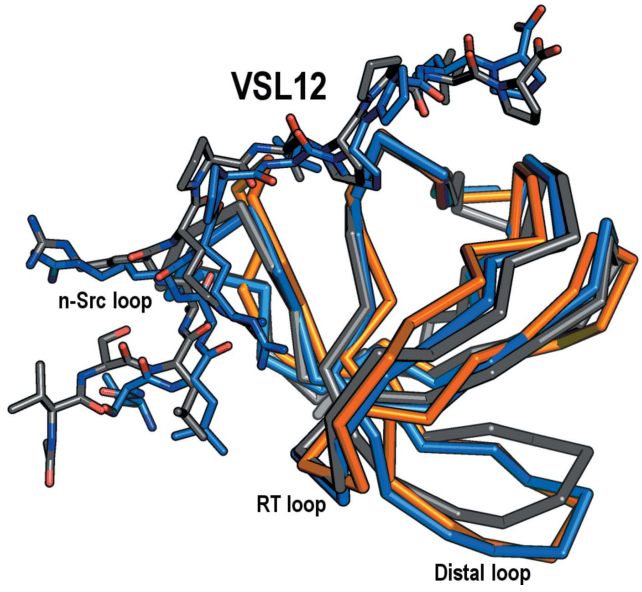

Figure 5
Superposition of the crystallographic VSL12 complex of the c-Src SH3 domain (dark grey) with that solved by NMR (PDB entry 1qwf; blue) and the unligated structure (PDB entry 1srl; orange).

displacement of Asp99 to optimize the formation of the salt bridge. As a consequence, the RT loop shows a different conformation compared with the SH3–APP12 complex. All of these changes result in an increase in the distances between Asp99 and Tyr92 (4.6 Å) and between $Arg6_{VSL12}$ and Tyr92 (6.3 Å) and in a larger distance between the tip of the RT loop and the n-Src loop (the distances between the Glu97 and Glu115 backbone CA atoms are 17.4 and 19.2 Å in the APP12 and VSL12 complexes, respectively; Fig. 4).

3.4. Comparison of the c-Src SH3 domain–VSL12 complex with previous structures

Comparison of the crystallographic structure of the c-Src SH3 domain–VSL12 complex (Src-SH3–VSL12) with the previously reported averaged minimized NMR structure of the Src-SH3–VSL12 complex (PDB entry 1qwf; Feng *et al.*, 1995) reveals a backbone r.m.s.d. of 1.11 Å for the whole SH3 domain. As in the APP12 complexes, the largest differences in the backbone between the crystallographic and the NMR structures are found in the distal loop (r.m.s.d. of >2.50 Å) located opposite to the binding site (Fig. 5). In this case, superposition of the residues of the peptide (1–12) results in a backbone r.m.s.d. of 1.55 Å.

Comparison of the crystallographic structure of the c-Src-SH3–VSL12 complex with the unligated c-Src-SH3 structure (PDB entry 1srl; Yu *et al.*, 1993) shows the same differences as described above in the comparison of the crystallographic APP12 complexes. In this case, the backbone superposition shows an r.m.s.d. of 1.94 Å and the movement of the n-Src loop is equivalent to that found in the APP12 complexes. The same differences in the position of the distal loop have also been found (Fig. 4).

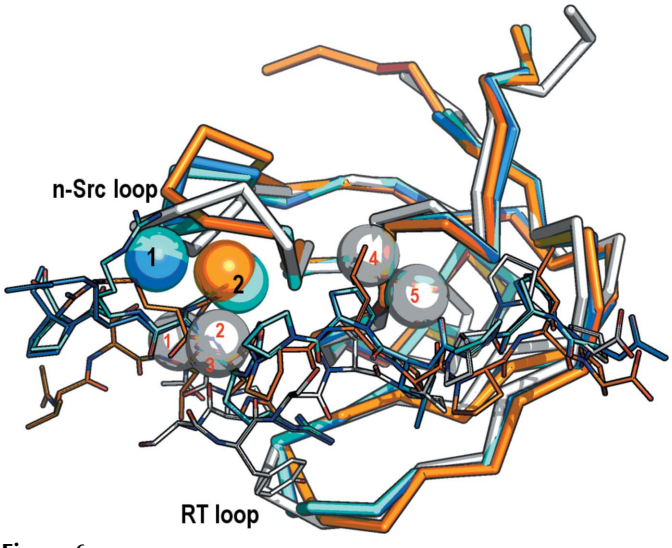

Figure 6
Water molecules at the binding interface of the c-Src SH3 domain in the APP12 (Thr98Asp, light blue; Thr98Glu, blue) and VSL12 (orange) complexes. The hydration spots are shown with the water molecules coloured the same as the protein. The hydration spots previously reported in the Abl-SH3 domain (PDB entry 1bbz; white) are also shown. The numbering of the hydration spots is the same as that previously reported by Palencia *et al.* (2010).

3.5. Water molecules in the APP12 and VSL12 complex structures of the c-Src SH3 domain

We have examined the presence of water molecules at the binding site in the crystallographic structures of the APP12 and VLS12 complexes of c-Src-SH3. In the APP12 complex structures with the Thr98Asp and Thr98Glu c-Src SH3 domain mutants only two water molecules are present in the binding interface in contact with residues of the peptide and the SH3 domain (Fig. 6): W1 is bound to Glu115 and $Arg9_{APP12}$, while W2 is bound to Asp117 and Pro6–$Asn8_{APP12}$. In the VSL12 complex the position of W1 is occupied by the side chain of $Arg5_{VSL12}$. W2 is also present at the interface of the VSL12 complex, but in this complex the water molecule is bound to Asp117 and $Arg6_{VSL12}$. All of these water molecules are practically buried at the interface of the binding site, with an accessible surface area (ASA) of less than 25 $Å^2$. The electron

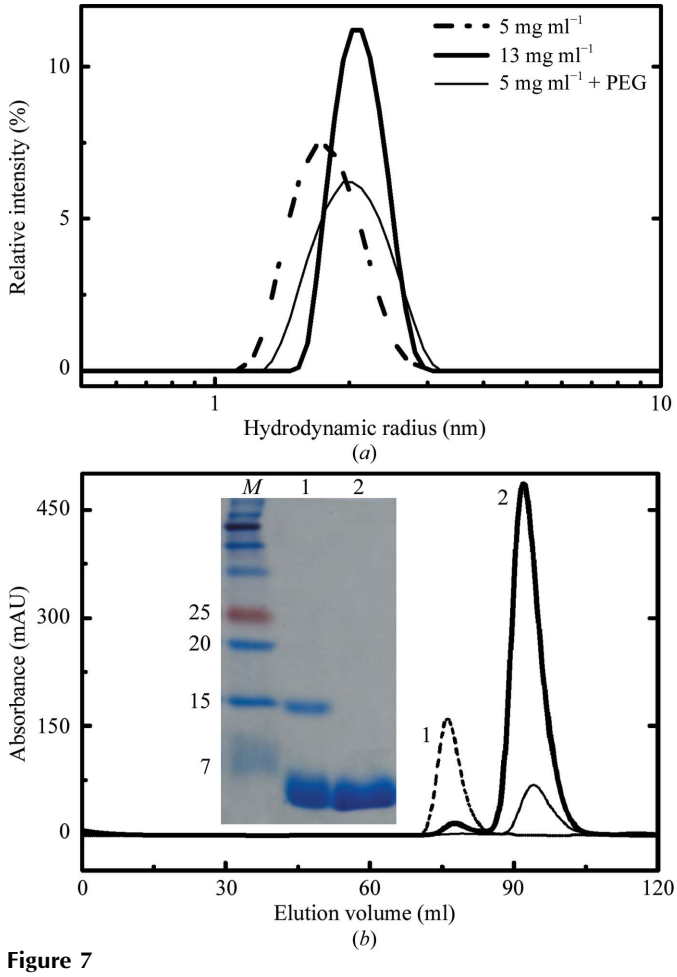

Figure 7
(*a*) Hydrodynamic radius (R_h) of the c-Src SH3 domain Thr98Glu mutant measured by DLS at different protein concentrations and in the presence of 5% PEG 300. (*b*) Size-exclusion chromatography of the c-Src SH3 domain Thr98Glu mutant (continuous line). Cytochrome *c* (molecular weight 13 kDa, dashed line) and Abl-SH3 (molecular weight 7.1 kDa, dotted line) were used as molecular-weight markers. The cross-linking experiment of the c-Src SH3 domain Thr98Glu mutant is shown in the inset: lane *M*, molecular-weight markers (labelled in kDa); lane 1, cross-linking experiment of the c-Src SH3 domain Thr98Glu mutant; lane 2, c-Src SH3 domain Thr98Glu mutant. The same results were obtained using the c-Src SH3 domain Thr98Asp mutant.

density for all these water molecules is well defined, with a σ level higher than 2.5 in the $2F_o - F_c$ difference map.

When we compared the water molecules present at the binding interface of the VSL12 and APP12 complexes with those in previous complexes of SH3 domains with PRMs, some important differences were observed. Taking as a reference the Abl-SH3–P41 structure (PDB entry 1bbz; Pisabarro & Serrano, 1996), which has been subjected to a detailed analysis of the water molecules that are buried upon binding (Palencia *et al.*, 2004, 2010), two different hydration spots are defined: one near to the 3_{10}-helix and the second near the n-Src loop (Martin-Garcia, Ruiz-Sanz *et al.*, 2012). Fig. 6 shows an overlay of the complexes of c-Src-SH3 and Abl-SH3 with PRMs, which clearly indicates the absence of water molecules at the 3_{10}-helix. It is worth noticing that W4 in the Abl-SH3 structure would be considered to be a structural water molecule as it is present in most of the unligated structures of the Abl-SH3 domain. Also, this water molecule is not in direct contact with the peptide in the complex structures (Cámara-Artigas *et al.*, 2007; Palencia *et al.*, 2010). However, the second hydration spot, near the n-Src loop, is also present in the c-Src SH3 domain structures, but is displaced by the different arrangement of the n-Src loop and the position of the flanking sequence of the PRMs.

Additionally, we have examined those water molecules which appear to be fully buried near the binding site. Interestingly, in the structure of the c-Src-SH3–VSL12 complex a fully buried water molecule (W9; ASA 0 Å^2) is located in a hydrophobic cavity formed by the residues Trp118, Pro133, Tyr92, Tyr131, Phe102 and Leu100. This water molecule is hydrogen bonded to the backbone atoms of Tyr131 (O, 2.73 Å) and Leu100 (N, 3.4 Å; O, 2.7 Å) and is at a distance of 7 Å from $Pro9_{VSL12}$. However, this water molecule does not appear in the c-Src-SH3–APP12 complex. This is a result of the displacement of Tyr92 into the hydrophobic pocket, which is caused by the formation of two hydrogen bonds from the latter to Asp99 and $Arg7_{APP12}$ (2.6 and 3.5 Å, respectively).

3.6. Oligomer formation

All of the crystallographic structures reported in this work have been solved from crystals obtained in the presence of PEG 300 at pH 5. Under these conditions, the crystal structure of the unligated c-Src SH3 domain shows the presence of an intertwined dimer stabilized by the presence of a PEG molecule (Cámara-Artigas, Martín-García *et al.*, 2009). However, the crystallographic structures of the complexes of the APP12 and VSL12 peptides show just one monomer of the SH3 domain bound to the peptide in the asymmetric unit.

To analyze the oligomer formation, we performed DLS experiments in the presence or absence of peptide and/or PEG 300 (Fig. 7*a*) at different protein concentrations. In the absence of additives, the dependence of the hydrodynamic radius (R_h) on the concentration obtained by means of DLS experiments indicates the presence of a monomer–dimer equilibrium in solution. At low protein concentrations R_h is about 1.8 nm, which corresponds to a monomer of the SH3 domain (Cámara-Artigas, Andújar-Sánchez *et al.*, 2009). However, at protein concentrations higher than 10 mg ml^{-1} the R_h value increases to 2.3 nm, which is close to the value reported for the c-Src SH3 dimer (∼2.5 nm; Cámara-Artigas, Martín-García *et al.*, 2009). The addition of 5% PEG 300 is sufficient to stabilize the formation of the dimer in solution and even at low protein concentrations (1 mg ml^{-1}) R_h values of 2.4 and 2.5 nm were obtained for the Thr98Asp and Thr98Glu mutants, respectively. The presence of a monomer–dimer equilibrium in solution was also confirmed by size-exclusion chromatography and cross-linking experiments (Fig. 7*b*).

4. Discussion

NMR spectroscopy and X-ray diffraction are the most powerful techniques for obtaining structural information from proteins. However, these techniques create models that have been fitted to different experimental data and therefore the models obtained by each technique are not expected to be identical. In fact, while the hydrophobic core of these models is almost the same, some serious differences can be found in the modelling of the flexible regions and in the side chains of residues at the surface. Nevertheless, molecular-dynamics simulation studies performed on protein structure models obtained by both techniques show that structures determined by means of X-ray diffraction are generally more suited for use as a starting point for modelling studies to investigate protein motion or protein–ligand interactions (Fan & Mark, 2003). Also, the accuracy of the crystallographic structures is higher when the resolution of the diffraction data is high. Finally, another advantage of crystallographic over NMR techniques in structural determination is the availability of information about the solvent.

In this work, we report the crystal structures of the complexes of the Thr98Asp and Thr98Glu mutants of the c-Src SH3 domain with two high-affinity peptides, APP12 and VSL12, at atomic resolution. Structures of the complexes of the wild-type protein have previously been reported using NMR techniques. The availability of structures solved using NMR and X-ray diffraction allows us to compare the structural information obtained using both techniques and to obtain additional information about the interactions of PRMs with the c-Src-SH3 domain.

No significant differences were found between the crystal structures of the Thr98Asp and Thr98Glu mutants complexed with the APP12 peptide. This result is in agreement with the previous mutational analysis of the c-Src SH3 domain, which indicates that the essential residues for ligand binding are Tyr90, Asn135 and Tyr136 in the first pocket, Tyr92, Trp118 and Pro133 in the second pocket and Asp99 and Tyr131 in the third pocket (Superti-Furga, 1995). Thr98Asp and Thr98Glu mutations do not affect the hydrogen-bond network or other interactions present in the binding interface of the complex and the crystal structures are practically identical. This result confirmed that Thr98 has a minor role in the binding affinity of PRMs.

We have also compared these crystallographic structures with the previous wild-type c-Src-SH3–APP12 complex and the unligated structures solved using NMR techniques. As expected, the hydrophobic cores of all of these structures are practically the same, while some important differences have been found in the positions of the loops. It is worth noting that in the c-Src SH3 domain the n-Src loop shows unusual flexibility and this feature might be key to its role as a hinge loop in the domain-swapping process that yields the intertwined structure (Camara-Artigas, Martin-Garcia *et al.*, 2009). Unexpectedly, major differences between the crystallographic and the NMR structures were found in the distal loop. These differences do not seem to be attributable to crystal contacts, as the crystal structures of the APP12 and VSL12 complexes belong to different space groups with dissimilar packing at the distal loop and the complex structures do not show noticeable differences in this loop.

The most important differences between the crystallographic and NMR structures are found in the peptides. The high resolution of the crystallographic structures allows very accurate modelling of the APP12 and VSL12 peptides. Also, as stated above, one of the advantages of these high-resolution crystal structures is the modelling of the water molecules. This information is important because the water molecules buried at the interface of SH3 domain–PRM complexes have been proposed to play a key role (Palencia *et al.*, 2010; Martin-Garcia, Ruiz-Sanz *et al.*, 2012). The crystallographic structures of the c-Src SH3 domain complexes allow us to analyze the presence of water molecules in their binding interface for the first time. A hydration spot at the 3_{10}-helix has been found in most SH3 domains; it was first described in the crystallographic structure of Abl-SH3 in complex with the synthetic high-affinity peptide P41 (Palencia *et al.*, 2010). When the crystallographic structures of the c-Src SH3 domain complexes are compared with those of Abl-SH3, no water molecule was found near to the 3_{10}-helix. Also, this water molecule is absent in some of the crystallographic structures of the Src family of tyrosine kinases (Martin-Garcia, Luque *et al.*, 2012). This absence would be explained by the $\sim$1 Å displacement found in the 3_{10}-helix compared with its position in the Abl-SH3 structures resulting from the substitution of the residue Cys100 in the Abl-SH3 by the bulkier Trp119 in the SH3 domains of the c-Src and Fyn SH3 domains (PDB entries 3fj5 and 3ua6; Cámara-Artigas, Martín-García *et al.*, 2009; Martin-Garcia, Luque *et al.*, 2012). A close inspection of the complex structures indicates that in the c-Src and Fyn SH3 domains the position occupied by the water molecule at the 3_{10}-helix is replaced by the hydroxyl group of the serine (Ser143 in the Src-SH3). In Abl-SH3 the side chain of this serine residue (Ser113) is hydrogen bonded to the backbone carbonyl of Gly97 in the n-Src loop and the resulting void space is filled by a water molecule.

The hydration spots described previously in the n-Src loop of the Abl-SH3–P41 complex (Palencia *et al.*, 2010) allow the number of contacts between the flanking sequence of the PRM and the SH3 residues to increase and play a role in the thermodynamic signature found for binding of PRMs to SH3 domains (Palencia *et al.*, 2004). A detailed analysis of these interactions is important because the determinant of the binding affinity and specificity has been attributed to the third binding pocket formed by the groove containing the RT and n-Src loops (Feng *et al.*, 1995). The differences arising from the comparison of the binding of the flanking sequences of the high-affinity peptides have been checked. APP12 and VSL12 were designed for the c-Src SH3 domain and both peptides have an arginine residue placed next to the canonical motif P*xx*P, which binds to Asp99 at the RT loop. P41 was designed for the Abl-SH3 domain (Pisabarro & Serrano, 1996) and this SH3 domain does not have positively charged residues flanking the P*xx*P canonical motif as there is not a partner negatively charged residue in the RT loop. Asp99, or the equivalent residue in the Src family of tyrosine kinases, plays a central role in the binding of the flanking sequence of the peptide and determines its orientation by the interaction with Arg or Lys residues present in the peptide. Besides the salt bridge, this positively charged residue can form a cation–π interaction with the aromatic residue at position 118. This specific conserved tryptophan residue has been proposed to determine the ability of some SH3 domains to bind peptides in different orientations (Trp119 in the Fyn-SH3 sequence; Fernandez-Ballester *et al.*, 2004). The orientation of this residue is not only determined by formation of the cation–π interaction but also by the formation of a hydrogen bond between the NE1 atom of the Trp118 side chain and the backbone O atom (Pro5 or Pro7 in the APP12 and VSL12 sequences, respectively). Asp99, or an equivalent residue, is not present in the Abl-SH3 sequence and the nature of the interaction between the RT loop and the peptide flanking sequence changes from a salt bridge to a hydrogen bond. In the P41 sequence Tyr4 is the key residue for the interaction of the peptide flanking sequence and its side chain forms several hydrogen bonds to residues in the RT loop of the Abl-SH3 domain. In addition, the backbone O atom forms a hydrogen bond to the NE1 atom of the side chain of Trp99 (equivalent to Trp118 in the c-Src sequence). All these interactions determine the situation of the flanking sequence of the PRM in the groove formed by the RT loop and the n-Src loop; the solvent plays a key role in increasing the interaction interface with the protein by filling the remaining space between the loops. In fact, in the VSL12 complex, in which the peptide fits better to the binding surface of the groove, only one water molecule has been found (accesible surface areas calculated using the *PISA* server: Src-SH3-T98E–VSL12, 534.1 Å^2; Src-SH3-T98D–APP12, 476.3 Å^2; Src-SH3-T98E–APP12, 474.5 Å^2).

The experiments performed to determine the oligomeric state of the c-Src SH3 domain in solution indicate that the c-Src SH3 domain shows some propensity to aggregate in solution by forming dimers. These oligomers are stabilized by the addition of low-molecular-weight PEGs to the solution and their presence is noticeable even at low protein concentrations. The stabilizing role of the low-molecular-weight PEGs is obvious if we take into account the crystallographic structure of the c-Src SH3 domain (Cámara-Artigas, Martín-García *et al.*, 2009). These crystals were obtained in the

presence of 5% PEG 300 and this molecule was present in the interface of the intertwined dimer. It is worth noting that the formation of a c-Src SH3 domain intertwined dimer in solution was previously predicted by molecular-dynamics simulation studies on amyloidogenesis (Ding *et al.*, 2002). Characterization of the aggregates present in solution under the conditions used to crystallize the protein was performed by means of DLS. In the absence of PEG the protein was a monomer, while a dimer was present in solution even at low protein concentrations in the presence of PEG (Cámara-Artigas, Martín-García *et al.*, 2009). The higher protein concentration assayed previously was 10 mg ml^{-1}; in this work, DLS measurements conducted at protein concentrations higher than 10 mg ml^{-1} revealed the presence of a dimeric species in solution even in the absence of low-molecular-weight PEGs (Fig. 7). Moreover, an increase in the polydispersity of the samples is observed as the protein concentration is raised. This indicates some kind of aggregation equilibrium in the solution. However, the addition of the APP12 and VSL12 peptides to the protein solution results in the formation of complexes in which a single molecule of the SH3 domain is bound to the peptide molecule. These observations are in agreement with the previously reported observation that addition of peptide greatly increases the stability of the domain (Feng *et al.*, 1994). Taking into account all of these results, we have proposed the presence of several equilibria in solution: the monomer–dimer equilibrium can be displaced by the presence of low-molecular-weight PEGs in the solution, but at the same time the addition of peptide competes with formation of the dimer.

Finally, the crystallographic structures of the high-affinity peptides APP12 and VSL12 described in this work provide more accurate information on the interaction of these PRMs with the SH3 domain of the Src family of tyrosine kinases. We have described the presence of several water molecules in the third pocket of the SH3 domain binding interface for the first time. The hydrogen bonds formed by these water molecules to residues in the flanking sequence of the PRMs contribute to the energetics of the binding. The results obtained from the crystallographic structures are key to understanding the driving forces for the binding of PRMs to SH3 domains and to characterizing the determinants of the high affinity of the VSL12 and APP12 peptides. Since tyrosine kinases comprise the largest group of oncoproteins (Rodrigues & Park, 1994), and given the important role of PRMs in the regulation mechanism and activity of these kinases, this knowledge will help in the rational design of high-affinity peptides to inhibit the interaction of the SH3 domains present in the tyrosine kinases with their target proteins.

This research was funded by the Spanish Ministry of Science and Innovation and Ministry of Economy and Competitiveness and FEDER (EU) (BIO2009-13261-C02-01/02 and BIO2012-39922-C02-01/02), the Andalusian Regional Government (Spain) and FEDER (EU) (P09-CVI-5063 and P10-CVI-5915). This work was performed by members of the research groups BIO-328 Protein Structures of the Andalusian Regional Government (Spain). We thank the XALOC beamline at Spanish Synchrotron Radiation Facility ALBA and Jordi Juanhuix and Jordi Benach for their assistance in the measurement of the crystals. We also thank beamline ID14-4 at the European Synchrotron Radiation Facility (ESRF) at Grenoble (France) for funding (MX-1225). We would also like to thank Professor Jose-Carlos Redondo-Olmedilla for revising the English text.

References

Adams, P. D. *et al.* (2010). *Acta Cryst.* D**66**, 213–221.
Afonine, P. V., Grosse-Kunstleve, R. W., Echols, N., Headd, J. J., Moriarty, N. W., Mustyakimov, M., Terwilliger, T. C., Urzhumtsev, A., Zwart, P. H. & Adams, P. D. (2012). *Acta Cryst.* D**68**, 352–367.
Benach, J., Cuní, G., Colldelram, C., Nicolás, J., Lidón, J., Gil-Ortiz, F. & Juanhuix, J. (2012). The 11th International Conference on Synchrotron Radiation Instrumentation, Lyon, France.
Cámara-Artigas, A., Andújar-Sánchez, M., Ortiz-Salmerón, E., Cuadri, C. & Casares, S. (2009). *Acta Cryst.* D**65**, 1247–1252.
Cámara-Artigas, A., Martín-García, J. M., Morel, B., Ruiz-Sanz, J. & Luque, I. (2009). *FEBS Lett.* **583**, 749–753.
Cámara-Artigas, A., Palencia, A., Martínez, J. C., Luque, I., Gavira, J. A. & García-Ruiz, J. M. (2007). *Acta Cryst.* D**63**, 646–652.
Cesareni, G., Gimona, M., Sudol, M. & Yaffe, M. (2006). *FEBS Lett.* **586**, 2606–2608.
Chen, V. B., Arendall, W. B., Headd, J. J., Keedy, D. A., Immormino, R. M., Kapral, G. J., Murray, L. W., Richardson, J. S. & Richardson, D. C. (2010). *Acta Cryst.* D**66**, 12–21.
DeLano, W. L. (2002). *PyMOL*. http://www.pymol.org.
Ding, F., Dokholyan, N. V., Buldyrev, S. V., Stanley, H. E. & Shakhnovich, E. I. (2002). *J. Mol. Biol.* **324**, 851–857.
Emsley, P. & Cowtan, K. (2004). *Acta Cryst.* D**60**, 2126–2132.
Emsley, P., Lohkamp, B., Scott, W. G. & Cowtan, K. (2010). *Acta Cryst.* D**66**, 486–501.
Evans, P. R. (2011). *Acta Cryst.* D**67**, 282–292.
Fan, H. & Mark, A. E. (2003). *Proteins*, **53**, 111–120.
Feng, S., Chen, J. K., Yu, H., Simon, J. A. & Schreiber, S. L. (1994). *Science*, **266**, 1241–1247.
Feng, S., Kasahara, C., Rickles, R. J. & Schreiber, S. L. (1995). *Proc. Natl Acad. Sci. USA*, **92**, 12408–12415.
Fernandez-Ballester, G., Blanes-Mira, C. & Serrano, L. (2004). *J. Mol. Biol.* **335**, 619–629.
Kabsch, W. (1976). *Acta Cryst.* A**32**, 922–923.
Kabsch, W. (2010*a*). *Acta Cryst.* D**66**, 125–132.
Kabsch, W. (2010*b*). *Acta Cryst.* D**66**, 133–144.
Kaneko, T., Sidhu, S. S. & Li, S. S. (2011). *Trends Biochem. Sci.* **36**, 183–190.
Kay, B. K. (2012). *FEBS Lett.* **586**, 2606–2608.
Krissinel, E. (2011). *Acta Cryst.* D**67**, 376–385.
Laskowski, R. A., MacArthur, M. W., Moss, D. S. & Thornton, J. M. (1993). *J. Appl. Cryst.* **26**, 283–291.
Laskowski, R. A. & Swindells, M. B. (2011). *J. Chem. Inf. Model.* **51**, 2778–2786.
Martín-García, J. M., Luque, I., Mateo, P. L., Ruiz-Sanz, J. & Cámara-Artigas, A. (2007). *FEBS Lett.* **581**, 1701–1706.
Martin-Garcia, J. M., Luque, I., Ruiz-Sanz, J. & Camara-Artigas, A. (2012). *Acta Cryst.* D**68**, 1030–1040.
Martin-Garcia, J. M., Ruiz-Sanz, J. & Luque, I. (2012). *Biochem. J.* **442**, 443–451.
Musacchio, A., Wilmanns, M. & Saraste, M. (1994). *Prog. Biophys. Mol. Biol.* **61**, 283–297.
Palencia, A., Camara-Artigas, A., Pisabarro, M. T., Martinez, J. C. & Luque, I. (2010). *J. Biol. Chem.* **285**, 2823–2833.
Palencia, A., Cobos, E. S., Mateo, P. L., Martínez, J. C. & Luque, I. (2004). *J. Mol. Biol.* **336**, 527–537.
Pisabarro, M. T. & Serrano, L. (1996). *Biochemistry*, **35**, 10634–10640.
Rodrigues, G. A. & Park, M. (1994). *Curr. Opin. Genet. Dev.* **4**, 15–24.

Scopes, R. K. (1974). *Anal. Biochem.* **59**, 277–282.
Superti-Furga, G. (1995). *FEBS Lett.* **369**, 62–66.
Terwilliger, T. C., Grosse-Kunstleve, R. W., Afonine, P. V., Moriarty, N. W., Zwart, P. H., Hung, L.-W., Read, R. J. & Adams, P. D. (2008). *Acta Cryst.* D**64**, 61–69.
Williams, J. C., Weijland, A., Gonfloni, S., Thompson, A., Courtneidge, S. A., Superti-Furga, G. & Wierenga, R. K. (1997). *J. Mol. Biol.* **274**, 757–775.
Winn, M. D. *et al.* (2011). *Acta Cryst.* D**67**, 235–242.
Yu, H., Rosen, M. K. & Schreiber, S. L. (1993). *FEBS Lett.* **324**, 87–92.